## **Materials Horizons**



## COMMUNICATION

**View Article Online** 

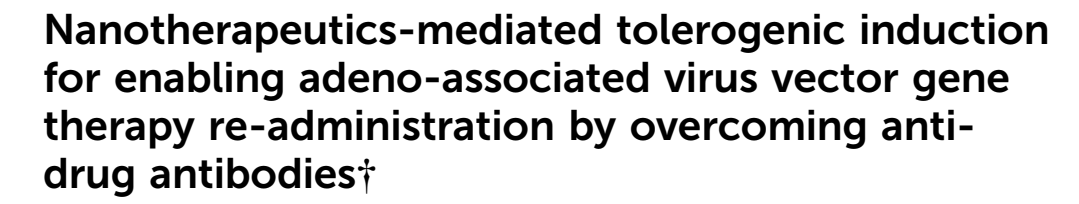


Cite this: Mater. Horiz., 2025, **12**, 6751

Received 3rd February 2025, Accepted 24th May 2025

DOI: 10.1039/d5mh00203f

rsc.li/materials-horizons



Yubo Liu,<sup>a</sup> Fangming Liang,<sup>a</sup> Rui Zhang,<sup>a</sup> Chengcheng Tang,<sup>b</sup> Xin Li,<sup>c</sup> 

Recombinant adeno-associated virus (AAV) vectors have become promising platforms to deliver therapeutic transgenes for the treatment of monogenic disorders. However, anti-AAV antibodies that are released by B cells after AAV treatment create a substantial barrier to their long-lasting safe and effective therapy, making AAV gene therapy a "one-shot" treatment. Herein, we developed tolerogenic nano-adjuvants (named RICP) composed of rapamycin (RAPA) and itaconate (ITA) to induce specific immune tolerance to overcome the anti-drug antibodies (ADAs). This strategy blocked the feedback loops of follicular helper T (Tfh) cells and germinal center B cells via metabolic regulation, complementary to the induction of regulatory T cells (Tregs) via mTORc1 inhibitor RAPA, consequently preventing the secretion of anti-AAV antibodies. The developed nano-adjuvants also significantly increased the expression of transgenes (such as luciferase, green fluorescent protein and human embryonic alkaline phosphatase reporter transgene) in the liver at re-dosing compared with mice treated with AAV alone, which showed almost no change in transgene expression. This emerging strategy provided an AAV re-administration schedule to not only mitigate toxicities with high vector doses but also re-store therapeutic benefits in children during significant cell proliferation.

## 1. Introduction

Recombinant adeno-associated virus (rAAV) vectors have become promising platforms to deliver therapeutic transgenes for monogenic disorders owing to their unique advantages such

#### New concepts

We propose a novel approach to block the Tfh-B cell axis while expanding Tregs to synergistically abolish memory humoral immune responses. By leveraging recent insights into the metabolic reprogramming of immune cells, we developed a nanoparticle-based tolerogenic adjuvant (RICP) comprising RAPA and itaconate (ITA). RICP, combined with an AAV8 vector, effectively eliminated anti-AAV antibodies and enhanced transgene expression in the liver upon AAV re-dosing. B cell-mediated immunity precludes re-administrations, making AAV gene therapy a "one-shot" treatment. A common approach to overcome this obstacle has been to use immunosuppressants, but it is associated with a high risk of infection. Swamping neutralizing antibodies with decoys enables the treatment of seropositive patients, but it is not efficient enough to overcome the high neutralizing antibody titers and is associated with an increased immunogenic risk. AAV capsid engineering can increase the number of subjects eligible for the first-time treatment, but this does not overcome the challenge of AAV re-administration. This study provided insights into the development of AAV gene therapy with higher efficacy and the establishment of a re-administration schedule suitable for re-storing therapeutic benefits in patients not only with initial treatment failure but also in the presence of significant cell proliferation, such as in children.

as the ability to transduce nondividing cells and long-term gene expression. However, B cell-mediated immunity precludes any re-administrations, making AAV gene therapy a "one-shot" treatment. Studies have shown that anti-AAV antibodies that are released by B cells after AAV treatment create a substantial barrier to their long-lasting safe and effective therapy.<sup>2-8</sup> In particular, anti-AAV antibodies neutralize the treatment by direct circulation clearance or activate the complement system by the formed immune complexes<sup>9,10</sup> (via binding antibodies with AAV vector), which further increases the processing of AAV by antigen-presenting cells (APCs) and the clearance of treated cells by CD8<sup>+</sup> cytotoxic T lymphocytes.<sup>3,4,7</sup> Furthermore, complement activation can trigger life-threatening inflammatory responses including thrombotic microangiopathy, acute kidney injury and immune-mediated myocardial inflammation. Most importantly, some of these activated B cells differentiate into

<sup>&</sup>lt;sup>a</sup> Wuya College of Innovation, Shenyang Pharmaceutical University, Shenyang, 110016, P. R. China. E-mail: liuhongzhuo@syphu.edu.cn, hezhgui\_student@aliyun.com, wangyongjun@syphu.edu.cn; Fax: +86 24 23986321; Tel: +86 24 23986321

<sup>&</sup>lt;sup>b</sup> Shenyang Sunshine Pharmaceuticals Co., Ltd., Shenyang, 110016, P. R. China

<sup>&</sup>lt;sup>c</sup> Department of Respiratory Medicine, First Affiliated Hospital of Jinzhou Medical University, Jinzhou, 121001, P. R. China

<sup>†</sup> Electronic supplementary information (ESI) available. See DOI: https://doi.org/ 10.1039/d5mh00203f

Communication **Materials Horizons** 

long-lived memory cells. A second encounter with the AAV results in the activation of memory B cells, leading to an enhanced and accelerated antibody response.<sup>2,8</sup>

A common approach to overcome this obstacle has been to use immunosuppressants for a long term to reduce B cell responses in humans; however, the evidence demonstrated that it is only partly effective and is associated with a high risk of infection. 11,12 The modified AAV vector by chemical coupling with polyethylene glycol has been shown to inhibit AAV neutralization. 13,14 Although multiple cycles of plasmapheresis can significantly reduce the total IgG level nonspecifically, ultimately it leaves the patients more vulnerable to infections.<sup>3,15</sup> Swamping neutralizing antibodies with decoys allows the treatment of seropositive patients, but this strategy is not efficient enough to overcome the high neutralizing antibody titers and is associated with an increased immunogenic risk.3,16 AAV capsid engineering can increase the number of subjects eligible for the first-time treatment, but this does not overcome the challenge of AAV re-administration. 17,18 A recently reported strategy to conjugate biologics to synthetic mannose polymers lowered antigenspecific T follicular helper cell and B cell responses, resulting in reduced anti-drug antibody (ADA) production. 19 The applicability of this strategy to AAV requires further verification for its safety and efficacy.

Of the techniques explored, inducing specific immune tolerance represents a promising strategy that has the potential to keep the normal immune response to the pathogens at a low immune burden. For instance, the rapamycin (RAPA)-loaded PLGA/PLA nanoparticles (NPs) have been investigated for inhibiting the formation of ADAs and AAV vector immune responses by selectively favoring the expansion and conversion of regulatory T cells (Tregs) via the immune tolerance-primed APCs. 20,21 Recent studies have highlighted that induced Tregs in the complex inflammation environment failed to maintain the immunosuppressive ability and even transformed into the effector T cells. 22-24 Hence, a strategy is needed to prevent other T cells (follicular helper cells, Tfh and T helper 2 cells, and Th2), many of which not only help in the formation and control selection of high-affinity germinal center B cells (GC B) but also function as critical regulators for the development of long-term humoral immunity via BGC cell differentiation to memory B cells and plasma cells (PCs).25-33

In the present study, we hypothesize that nanoparticles that both induce dendritic cell (DC)-Treg axis and inhibit Tfh-B cell axis could overcome the immunity barrier of AAV readministration. Since metabolic reprogramming in immune cells following activation is a recently appreciated regulator of their development and differentiation, we chose the combination of RAPA and itaconate (ITA) to be tolerogenic adjuvants. Specifically, the mammalian target of rapamycin (mTOR) consists of two distinct protein complexes, mTORc1 and mTORc2, which can inhibit Treg differentiation by suppressing Foxp3 expression.<sup>34–36</sup> mTOR blockade by RAPA primarily inhibits mTORc1 to promote the generation of Tregs but seems to cause secondary activation of mTORc2, which favors the expansion of Tfh cells. 37,38 Another important issue is that mTOR is expressed ubiquitously in many

cells. Environmental factors might override the intrinsic effect of the RAPA on helper CD4<sup>+</sup> T cells, whose normal helper T cell responses may have been mediated by other types of cells such as innate immune cells. Furthermore, during initial activation, T helper cells are more dependent on glycolysis, whereas Treg cells mainly rely on fatty acid oxidation for their function. 39-42 Therefore, inhibition of glycolysis can inhibit the proliferation of T helper cells including Tfh cells and Th2 cells without blocking Tregs. ITA and its derivations have been recently shown to inhibit glycolysis, block reactive oxygen species production and inhibit Janus kinase 1 activation. 43-52 The resulting immune toleranceinducing NPs ingeniously integrated both RAPA and ITA into the facile carrier-free nano-system via coacervation technique and abolished the undesired immune response during AAV treatment by inducing synergistic effects on cellular regulatory pathways.

## Materials and methods

#### 2.1 Materials

RAPA was obtained from Xi'an Qiyue biotechnology Co. Ltd. Itaconic anhydride, decanoic acid, myristic acid, stearic acid, 4decenoic acid, 9-decenoic acid, decanedioic acid, decyl alcohol, myristyl alcohol and stearyl alcohol were obtained from Aladdin Biochemical Technology Co. Ltd (Shanghai, China). TMB twocomponent substrate solution and keyhole limpet hemocyanin (KLH) were obtained from Beijing Solarbio Science & Technology Co., Ltd. Ovalbumin was obtained from Sigma-Aldrich. Uricase was obtained from MACKLIN. AAV8-luciferase (AAV8-Luc), AAV8-green fluorescent protein (AAV8-GFP) and AAV8-Human embryonic alkaline phosphatase reporter transgene (AAV8-SEAP) were obtained from WZ Biosciences Inc. Glass bottom cell culture dishes, cell culture dishes and plates were purchased from Wuxi NEST Biotechnology Co., Ltd, China.

#### 2.2 Synthesis of RAPA-aliphatic acid

A typical synthesis example is provided herein for RAPA-decanoic acid. A mixture of decanoic acid and excess vinyl acetate was placed in a reaction flask degassed with nitrogen. The catalyst ([Ir(cod)Cl]<sub>2</sub>) and sodium acetate were added into the reaction flask at 110 °C for 24 h. The reaction mixture was moved into cold water and extracted with dichloromethane. Then, a mixture of RAPA, vinyl decanoic acid and Novozyme 435 in methylbenzene was stirred at 45 °C for 48 h. The concentration and purification were determined by silica gel flash chromatography with dichloromethane-methanol (20:1) as the eluant. The other compounds synthesized according to the above methods are as follows: RAPA coupled with myristic acid (RAPA-C<sub>14</sub>), stearic acid (RAPA-C<sub>18</sub>), 4decenoic acid (RAPA-C<sub>10(4)</sub>), 9-decenoic acid (RAPA-C<sub>10(9)</sub>) and decanedioic acid (RAPA-C<sub>10(COOH)</sub>).

#### 2.3 Synthesis of ITA-aliphatic alcohols

A typical synthesis example is provided herein for ITA-stearic alcohol. Stearyl alcohol was introduced in a glass flask at 110 °C. Then, equimolar itaconic anhydride was added. The reaction mixture was kept under magnetic stirring at 110 °C for

150 min. The reaction mixture was poured in cold heptane. White crystals of ITA-stearic alcohol were obtained. The other compounds synthesized according to the above-mentioned methods are as follows: ITA coupled with decyl alcohol ( $-C_{10}$ ) and myristyl alcohol (ITA-C<sub>14</sub>).

#### 2.4 Preparation of co-assembled NPs

The coacervation technique adopted was to disperse the sodium salt of ITA-C<sub>18</sub> into an aqueous solution in the presence of 1% polyvinyl alcohol (PVA; Sigma Cat.360627) at an appropriate temperature, and to dissolve the RAPA-C<sub>10</sub> with ethanol. The two solutions were mixed to form a single-phase solution. A selected coacervating solution (Dilute hydrochloric acid) was then added drop-wise until reaching pH 4.0. The obtained suspension was then poured in a cold water bath at 15 °C.

#### 2.5 In vivo biodistribution

RAPA-Fluorescence (RAPA-Flu) probe was synthesized similarly to the methods in Section 2.2. Specifically, we first synthesized RAPA-C<sub>10(COOH)</sub>. Then, 5-aminofluorescein was coupled to the carboxyl group of the RAPA-C<sub>10(COOH)</sub> via a simple amide reaction, and RAPA was modified with fluorescein. Then, by the coacervation technique discussed in Section 2.4, RAPA-Flu was used to co-assemble with ITA-C<sub>18</sub> to form R<sub>Flu</sub>I<sub>18</sub>CP. R<sub>Flu</sub>I<sub>18</sub>CP and free RAPA-Flu were intravenously injected into mice, respectively. After 2 h, 6 h and 24 h post-injection, the major organs of mice were harvested for analysis using an in vivo imaging system (IVIS).

#### 2.6 Cytotoxicity assay

Human umbilical vein endothelial cells (HUVECs) and RAW264.7 cells were seeded into 96-well plates, respectively, at a density of  $5 \times 10^3$  cells per well and incubated for 24 h in a cell incubator (37 °C, 5% CO<sub>2</sub>). Then, serial dilutions of RAPA solution, ITA- $C_{18}$  solution and RICP were added into wells. After incubation for 24 h, a CCK8 solution was added to the 96-well plate. After further 1 h incubation, the absorbance was measured at 450 nm.

To evaluate the potential hepatotoxicity, C57BL/6 mice were administered with RICP intravenously at therapeutic doses every other day for a total of five days. Serum samples were subsequently collected for the measurement of alanine aminotransferase (ALT) and aspartate aminotransferase (AST) activities.

## 2.7 Isolation of BMDCs and tolerogenic induction in vitro

On day 0, bone marrow cells were isolated from the femur and tibia of C57BL/6 mice. The cell medium contained 2-mercaptoethanol, recombinant mouse GM-CSF and recombinant mouse IL-4. On day 2 and day 4, the medium and cytokines were replaced with fresh ones. Bone marrow-derived dendritic cells (BMDCs) were collected on day 7.

BMDCs were planked in a 12-well plate at a density of  $1 \times 10^6$  cells per well. For NP uptake evaluation,  $R_{\rm Flu}$ ICPs or free RAPA-Flu was incubated with BMDCs for 6 h. Then the nuclei were stained with Hoechst 33342. The results were examined using a confocal laser scanning microscope and a

flow cytometer. For tolerant dendritic cell (tolDC) induction, BMDCs were co-cultured with different components (equimolar RAPA at a concentration of 100 nM and ITA-C18 at a concentration of 250  $\mu M$ ) for 4 h and then activated by LPS  $(100 \text{ ng mL}^{-1})$  for 24 h. CD40, anti-CD80, anti-CD86, MHC II and IL-10 of treated BMDCs were examined by flow cytometry to determine the efficacy of immune tolerance.

Naïve CD4<sup>+</sup> T cells were isolated from the spleen of Balb/c mice and purified using a MojoSort™ Mouse CD4 Naïve T Cell Isolation Kit (BioLegend, 480039). Purified T cells were stained with 5,6-carboxyfluorescein diacetate (CFSE) and co-cultured with BMDCs pre-treated with different treatment formulations for 3 days. The proliferation results were examined using a flow cytometer. Naïve CD4 $^+$  T cells (1 imes 10 $^5$  cells per well) and  $R_{10}I_{18}CP$  pre-treated BMDCs (1  $\times$  10<sup>4</sup> cells per well) were co-cultured in the presence of soluble anti-CD3E, anti-CD28 and recombinant mouse IL-2 (Cat. No.: CK24; Novoprotein, Shanghai, China) for 5 days. Then, mixed lymphocytes were stained with fluorochrome-conjugated anti-mouse Foxp3 and examined using a flow cytometer.

For Th2 differentiation, naïve CD4<sup>+</sup> T cells were co-cultured with soluble anti-CD3E, anti-CD28, recombinant mouse IL-2, recombinant mouse IL-4 and recombinant mouse IFN-γ. Meanwhile, CD4<sup>+</sup> T cells were treated with various components for 5 days. In vitro-differentiated CD4 T cells were incubated with a cell stimulation cocktail (eBioscience, 00-4975-93) for 4 h and stained with eFluor 450 anti-IL13 antibodies and APC anti-IL4 antibodies for intracellular cytokine staining analysis.

#### Specific immune tolerance induced by RICP

To determine preferred formulations in our research studies, we chose uricase as a model antigen, an enzyme limited by immunogenicity. For the uricase experiment, the uricase-alone control group and all other treated groups were injected with 625  $\mu g \ kg^{-1}$  uricase per animal every 7 days. We set up four free drug control groups: (1) ITA group (50 mg kg<sup>-1</sup>, three times every 7 days), (2) RAPA group (5 mg kg<sup>-1</sup>, three times every 7 days), (3) RAPA + ITA group (RAPA 5 mg kg $^{-1}$  and ITA 50 mg kg $^{-1}$ , three times every 7 days) and (4) RAPA-C<sub>10</sub> + ITA-C<sub>18</sub> group (RAPA 5 mg kg<sup>-1</sup> and ITA 50 mg kg<sup>-1</sup>, three times every 7 days). Then, we wanted to know the significance of nano-design for the therapeutic effect of RAPA-C<sub>10</sub> + ITA-C<sub>18</sub>, so RICP group (equal to 5 mg kg<sup>-1</sup> RAPA and 50 mg kg<sup>-1</sup> ITA, once every 7 days), was added. Sampling and injection timing are indicated in figures legends.

To determine whether RICP could induce antigen-specific immunological tolerance, we assessed whether mice tolerized to KLH by RICP would maintain a normal immune response to OVA. C57BL/6 mice were divided into two groups: KLH group and KLH + RICP group. The KLH group was injected with KLH  $(5 \text{ mg kg}^{-1})$  per animal every 7 days. The KLH + RICP group was injected with KLH (5 mg kg<sup>-1</sup>) and RICP (equal to 5 mg kg<sup>-1</sup> RAPA and 50 mg kg<sup>-1</sup> ITA, once every 7 days) per animal every 7 days. After three times, both groups were re-challenged three times with KLH and OVA on day 21, day 28 and day 35. Sampling is indicated in figure legends.

Communication Materials Horizons

Antibody levels were measured by indirect ELISA. Stripwell microplates (Costar) were coated with 100  $\mu$ L of KLH at 5  $\mu$ g mL<sup>-1</sup>, OVA at 10  $\mu$ g mL<sup>-1</sup>, and uricase at 1  $\mu$ g mL<sup>-1</sup>, respectively. Nunc maxisorp plates (Invitrogen) contain 1  $\times$  10<sup>9</sup> viral genomes per well. HRP-conjugated goat anti-mouse IgG (abcam) and HRP-conjugated goat anti-mouse IgM (ZSGB-BIO) were used to detect IgG and IgM antibodies, respectively. The optical density (OD) of the wells was read at a wavelength 450 nm. A four-parameter logistic curve-fit graph was prepared with the dilution on the *x*-axis (log scale) and the OD value on the *y*-axis (linear scale) for each sample. The area under the curve (AUC) for each sample was determined by the OD value on the *y*-axis (linear scale) *versus* the dilution on the *x*-axis (log scale).

#### 2.9 AAV8 efficacy studies by RICP

C57BL/6 mice were injected first using an AAV8 vector encoding Luc together with RICP on day 0, followed by the second administration of an AAV8 vector encoding for Luc to monitor the transgene expression level by IVIS imaging and the activity of Luc by luminescence or the second administration of an AAV8 vector encoding for the green fluorescent protein (GFP) to visualize transgene expression in the liver. RICP (equal to 5 mg kg<sup>-1</sup> RAPA and 50 mg kg<sup>-1</sup> ITA) was dosed when co-administered with a vector dose of  $4 \times 10^{12} \text{ vg kg}^{-1}$  AAV8. Enzymatic Luc activity was measured using a Promega Luciferase Assay System. Specifically, the mice were euthanized, and equal liver tissues were weighed on day 21 and day 42. The ONE-Glo™ Buffer from the ONE-Glo™ Luciferase Assay System was transferred into the ONE-Glo™ Substrate vial and mixed by inversion until the substrate was completely dissolved. The lysed liver tissue was diluted 10 folds, mixed thoroughly with the assay reagent, and transferred to a 96-well opaque white plate. After incubation for 3 minutes, the luminescence signal was measured using a luminometer.

SEAP is a reporter protein that is secreted into the extracellular space and detected by testing serum, leaving animals healthy for further experimentation. C57BL/6 mice were injected first with an AAV8 vector encoding SEAP (4  $\times$   $10^{12}$  vg kg $^{-1}$ ) together with RICP on day 0, followed by the second administration of an AAV8 vector encoding SEAP with RICP on day 21. Sampling was done weekly to monitor the anti-AAV8 IgG anti-body and SEAP. Besides, anti-AAV8 IgM antibody on day 7 and transcription of the mRNA on day 42 were detected. The SEAP reporter gene activity was measured using a Phospha-Light SEAP Reporter Gene Assay System (Invitrogen).

All animal experiments were approved by the Animal Laboratory Ethics Committee of Shenyang Pharmaceutical University and performed under the guidelines for the care and use of laboratory animals.

For RNA extraction, reverse transcription and qPCR, livers were harvested from mice, lysed using Trizol Reagent, snap-frozen in liquid nitrogen, and stored at  $-80\,^{\circ}\text{C}$  until processing. Tissues were homogenized in Trizol using a homogenizer. Reverse transcription and quantitative PCR (qPCR) analyses were performed. The quantification of the transcript was performed using a  $2-\Delta\Delta\text{C}$ t method with internal reference genes.

#### 2.10 Detection of anti-AAV neutralizing antibodies (Nab)

HEK-293T cells were seeded into 96-well plates at a density of  $1 \times 10^4$  cells per panel and incubated for 12 h. Serum samples at week 6 from the AAV-SEAP experiments were heated at 56 °C for 30 minutes and diluted in fetal bovine serum (FBS) in a range of ratios. The AAV-Luc vector was diluted in DMEM and added to each serum tube with a multiplicity of infection of 1  $\times$ 106 for AAV-Luc. The virus was mixed with diluted serum obtained from untreated mice as a positive control for Luc expression. The mixtures were incubated for 1 h at 37 °C. After incubation, an rAAV-serum complex was transferred to the plated cells and incubated for 24 h. The level of anti-AAV NAb was measured using a Luciferase Reporter Gene Assay Kit (Beyotime). $^{53,54}$  We also injected the mixture of AAV-Luc (1 imes $10^{11} \text{ vg mL}^{-1}$ , 20 µL) and undiluted serum (20 µL) into mice. Seven days later, by administering p-luciferin potassium salt and anesthetics to the mice, we observed their luciferase transfection status using an in vivo imaging system (IVIS).

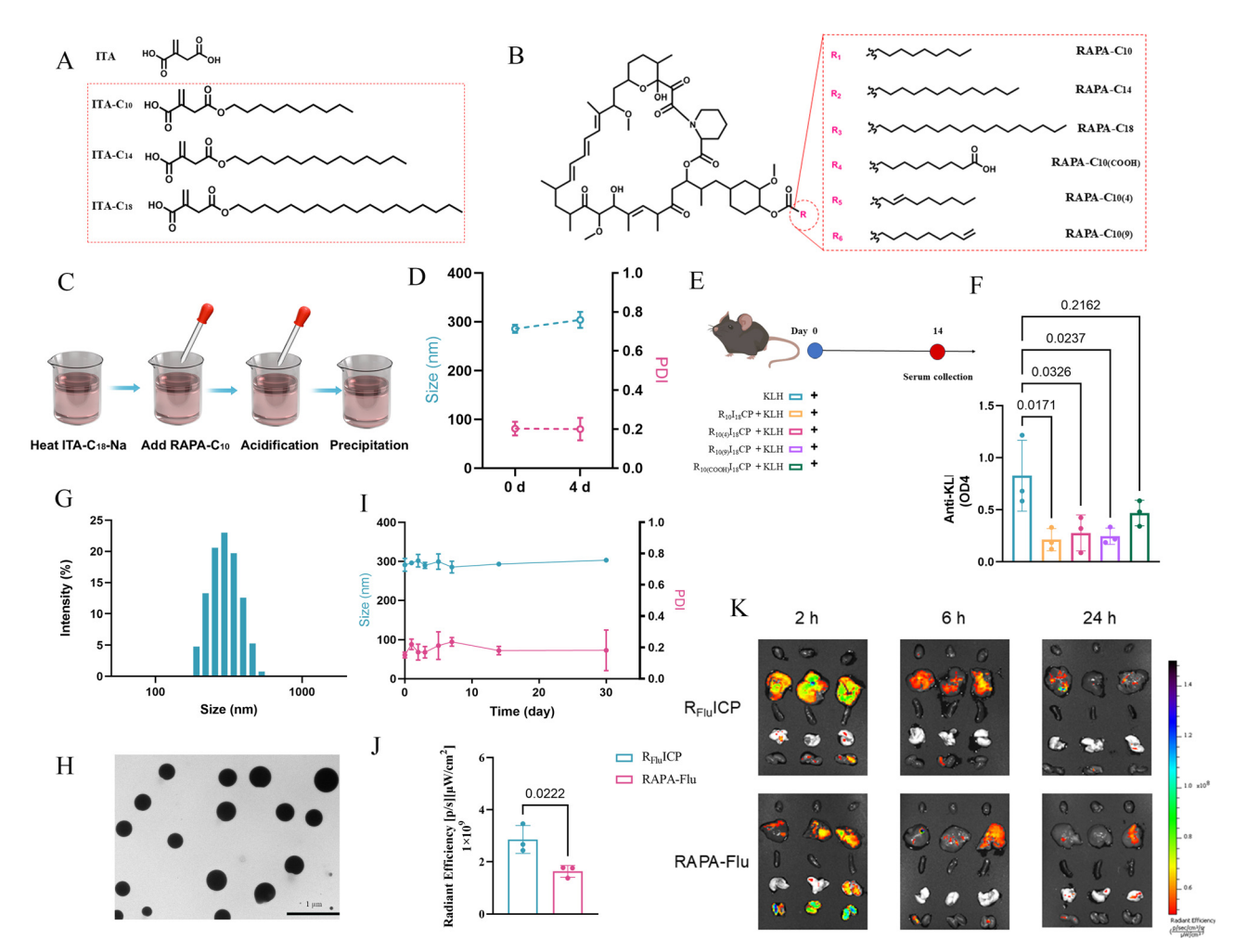
#### 2.11 Statistical analysis

Statistical analysis was performed using GraphPad Prism 9. The analysis of statistical significance between two groups was assessed using a two-tailed unpaired *t*-test. For multiple group comparisons, one-way or two-way ANOVA with Tukey's multiple comparison test was performed.

## 3. Results

#### 3.1 Preparation and characterizations of RICP

The nanoscale particulate form is an ideal strategy to specifically deliver ingredients to APCs, as these cells are experts in capturing and internalizing little pellets. Thus, we first evaluated whether 4octyl itaconate (4-OI), an endogenous ITA mimic, was coassembled with RAPA by the coacervation technique. The advantage of the coacervation technique is that it avoids toxic organic solvents in the production process. Unfortunately, 4-OI alone could not be successfully prepared into co-assembled nanoparticles, which may be due to its unsuitable amphipathic property. Hence, we synthesized ITA-C<sub>10</sub> and ITA-C<sub>14</sub> sequentially, and ITA-C<sub>18</sub> ultimately (Fig. 1(A) and Fig. S1, ESI†). ITA-C<sub>18</sub> can complete self-assembling due to its stronger hydrophobic force, whereas cannot co-assemble with RAPA. Likewise, we modified RAPA-C<sub>10</sub>, RAPA-C<sub>14</sub> and RAPA-C<sub>18</sub>, respectively (Fig. S2, ESI†), to fabricate co-assembled nanoparticles in pairs with ITA-C18 (Fig. 1(B) and (C)) and named  $R_{10}/I_{18}CP$ ,  $R_{14}/I_{18}CP$  and  $R_{18}/I_{18}CP$ I<sub>18</sub>CP. The stability of these NPs was evaluated in PBS containing 10% FBS at pH 7.4 and under 37  $^{\circ}$ C. The results showed that  $R_{14}/$ I<sub>18</sub>CP precipitated crystals rapidly, the particle size and polydispersity index (PDI) of R<sub>18</sub>/I<sub>18</sub>CP were significantly increased within 4 days and only R<sub>10</sub>/I<sub>18</sub>CPs exhibited preferable colloidal stability as to their minimal variation of the mean diameter and PDI (Fig. 1(D) and Fig. S3, S4, ESI†). Next, based on the structure of RAPA-C<sub>10</sub>, we subsequently modified RAPA with 4-decenoic acid, 9-decenoic acid and decanedioic acid and separately named RAPA- $C_{10(4)}$ , RAPA- $C_{10(9)}$ , and RAPA- $C_{10(COOH)}$  (Fig. 1(B)). The



 $\textbf{Fig. 1} \quad \text{Characterization of RICP. (A) Structures of ITA-$C_{10}$, ITA-$C_{14}$ and ITA-$C_{18}$. (B) Structures of RAPA-$C_{10}$, RAPA-$C_{14}$, RAPA-$C_{18}$, RAPA-$C_{10(4)}$, RAPA-$C_{18}$, RAPA-$C_{18}$,$  $C_{10(9)}$  and RAPA- $C_{10(COOH)}$ . (C) Preparation process of RICP. (D) Hydrodynamic sizes and PDI of  $R_{10}I_{18}$ CP. (E) C57BL/6 mice injected intravenously once with KLH alone (100 μg) or with KLH + RICP (R<sub>10</sub>I<sub>18</sub>CP, R<sub>10(COOH)</sub>I<sub>18</sub>CP, R<sub>10(4)</sub>I<sub>18</sub>CP and R<sub>10(9)</sub>I<sub>18</sub>CP, respectively). (F) Anti-KLH IgG antibody levels determined on day 14 using ELISA (n = 3). (G)–(I) Size, TEM and long-time stability of RICP, respectively. (J) In vivo biodistribution of R<sub>FIII</sub>ICP and RAPA-Flu solutions at 2 h. (K) Ex vivo imaging of major organs.

structures of all the above-mentioned new compounds were confirmed by LC-MS and <sup>1</sup>H NMR (Fig. S5-S19, ESI†). Expectedly, there was no significant difference in the mean diameter and PDI of these four NPs (Fig. S20, ESI†). We implemented a simplified pharmacodynamic study by intravenous injection of KLH concomitantly with NPs (Fig. 1(E)). Indeed, the KLH-specific IgG antibody responses were strongly decreased in R<sub>10</sub>/I<sub>18</sub>CP, R<sub>10(4)</sub>/  $I_{18}$ CP and  $R_{10(9)}/I_{18}$ CP compared to vehicle control mice except for  $R_{10(COOH)}/I_{18}CP$  (Fig. 1(F)). Considering the easy oxidation of unsaturated bonds, we finally chose RAPA-C10 and ITA-C18 as the preferred components to prepare CPs, named RICP. As shown in Fig. 1(G) and (H), RICP had a spherical structure with an average particle size of 321.5  $\pm$  15.44 nm and a zeta potential of  $-1.78 \pm 0.09$  mV (Table S1, ESI†). This near-neutral surface charge reflected the dense PVA layer on the particle surface, which effectively shielded any underlying charge, allaying any concerns about colloidal stability. The long-time storage stability of RICP was evaluated for 30 days at 4 °C, and the size and PDI are recorded in Fig. 1(I). Next, we synthesized RAPA coupled with 5-aminofluorescein (RAPA-Flu) to prepare R<sub>Flu</sub>ICP for monitoring the in vivo fate of NPs (Fig. S21 and S22, ESI†). The biodistribution of R<sub>Flu</sub>ICP in main tissues was investigated and detected using an *in vivo* imaging system (IVIS) at different time points. As shown in Fig. 1(J) and (K), R<sub>Flu</sub>ICP showed stronger fluorescence signals in the liver after intravenous injection compared with the RAPA-Flu solution. These results suggested that the nanoparticulate form could significantly enhance the accumulation in the liver of  $R_{Flu}ICP$ .

#### 3.2 Cellular uptake and tolerogenic induction in vitro

We used in vitro monocyte-derived DC differentiation models (denoted BMDCs, Fig. 2(A)) to compare the uptake of free versus nanoparticle-formulated rapamycin. Immature BMDCs were incubated with either free RAPA-Flu or RFIuICP at 37 °C for 6 h, and cellular internalization was first visualized by confocal microscopy (Fig. 2(B)) and then quantified by flow cytometry (Fig. 2(C)). BMDCs treated with R<sub>Flu</sub>ICP showed markedly brighter intracellular green fluorescence than those treated

Communication **Materials Horizons** 

with free RAPA-Flu, demonstrating that the nanoparticle formulation greatly enhances uptake efficiency.

Unlike free rapamycin, which must enter cells via passive diffusion and thus show relatively low and variable uptake, R<sub>Flu</sub>ICP nanoparticles are taken up actively by DCs and macrophages through scavenger receptors, and complement receptormediated endocytosis. Their pathogen-mimetic size and surface complement opsonization promoted efficient recognition and internalization, ensuring a higher intracellular delivery of cargo than the free drug.

Commonly, DCs with a stable, semi-mature phenotype and tolerogenic attributes are designated as tolerogenic DCs

(tolDCs). To investigate whether RICP can induce tolDC, immature BMDCs (iDCs) were cultured in the presence of various formulations for 4 h and subsequently activated by LPS for 24 h into mature BMDC state (mDCs) (Fig. 2(A)). It means that if RICP had the ability to induce immune tolerance, the costimulatory signal of mDCs will be suppressed. Flow cytometry analysis indicated that mDCs expressed costimulatory surface molecules (CD80, CD86 and CD40) and MHC II at higher levels than iDCs (Fig. 2(D)-(G)). The costimulatory molecule levels of free RAPA- and RICP-treated BMDCs were significantly lower than those of mDCs. In addition, free ITA-C<sub>18</sub> did not affect costimulatory markers. IL-10 of RICP-treated BMDCs presented

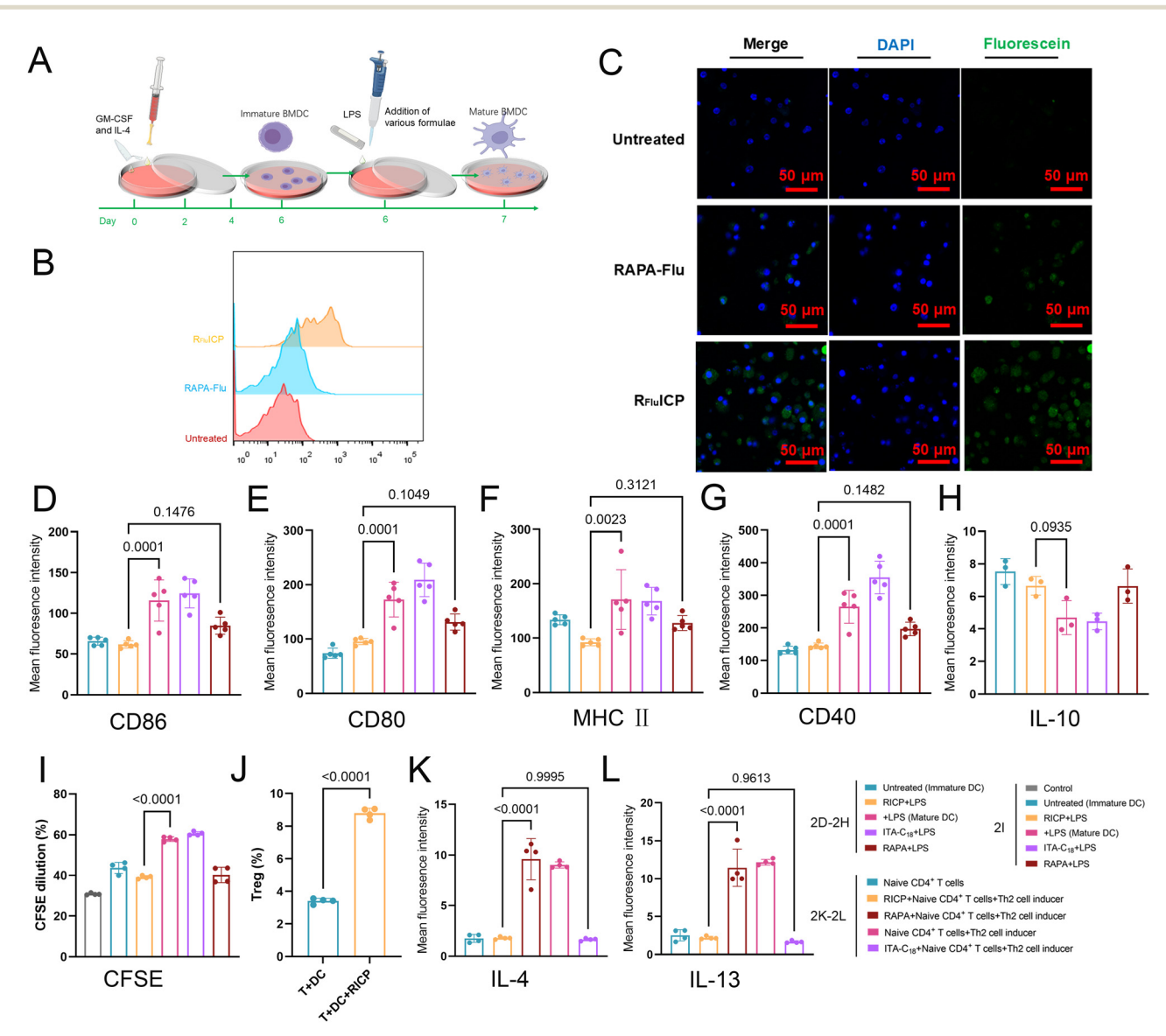


Fig. 2 RICP-mediated induction of toIDCs and subsequent evaluation of Th2 cells in vitro. (A) Schematic showing in vitro DC cultures of C57BL/6 bone marrow progenitor cells in the presence of GM-CSF and IL-4, leading to the differentiation of precursors into BMDCs. (B) Flow cytometry measurements of immature BMDCs after incubation with free RAPA-Flu and  $R_{Flu}$ ICPs for 6 h, respectively. (C) Confocal microscopic images of immature BMDCs after incubation with free RAPA-Flu and  $R_{Flu}ICPs$  for 6 h, respectively. Scale bar = 50  $\mu$ m. (D)-(G) BMDC maturation marker assay (CD86, CD80, MHC II and CD40) using flow cytometry. (H) Secretion of IL-10 by BMDCs after the addition of various formulations. (I) RICP-treated BMDCs and sorted naïve CD4+T cells (pre-stained by CFSE) were cocultured for 72 hours in MLR (J) Gated Foxp3<sup>+</sup> cells in T cells cultured with or without RICP-treated BMDCs. (K) and (L) Th2 cytokines (IL-4 and IL-13) released via the addition of various formulations of pulsed naïve CD4<sup>+</sup> T cells.

a slightly raised trend compared to the mDC group although it was not a significant difference (Fig. 2(H)). It might attribute to possible insufficient time for incubation. Next, T cell proliferation was investigated by mixed leukocyte reaction (MLR) to indirectly determine the tolerogenic property of BMDCs treated with various formulations. Both RICP- and free RAPA-treated BMDCs induced less T cell proliferation (~38%) than mDCtreated T cells ( $\sim 60\%$ ) but induced comparable proliferation to that induced by iDC-treated T cells (~40%) (Fig. 2(I)). This indicated that RAPA in RICP is the main ingredient of inducing tolDC in phenotypic or proliferation experiments rather than ITA. Furthermore, T cells with RICP-treated BMDC cultures contained significantly higher proportions of regulatory T cells (Foxp3<sup>+</sup> cells) compared to mDC-treated T cell cultures (Fig. 2(J)). Collectively, RICP can induce to LDC in vitro and further promote Treg maturation.

T follicular helper (Tfh) cells located in B cell follicles are known to provide help for the formation and maintenance of germinal center B cell reactions. Tfh cells produce the Th2 signature cytokine IL-4, indicating that Tfh cells and Th2 cells display similar phenotypical and functional properties, and both helper T cell subtypes are critical partners to exert full B cell function. 55,56 Since it is difficult to get in vitro real Tfh cells, only Th2 cells were used to evaluate RICP in vitro. Th2 cells mediated the activation and maintenance of humoral immune responses against extracellular antigens by producing various cytokines such as IL-4, IL-5, and IL-13. Therefore, to verify whether ITA can inhibit Th2 cell differentiation, we sorted naïve CD4<sup>+</sup> T cells, added suitable agents and examined the proportion of Th2 cells in total T cells by flow cytometry. The results indicated that the ITA-C<sub>18</sub> and RICP groups can effectively inhibit the differentiation and maturation of naïve CD4<sup>+</sup> T cells into Th2 cells instead of the free RAPA group (Fig. 2(K) and (L)). It may be due to mTORc2, which is indispensable for Th2 differentiation, whereas mTOR blockade by RAPA seems to primarily affect mTORc1 and might cause secondary activation of mTORc2.34-36 Thus, it may not be adequate for RAPA alone to inhibit Th2 differentiation.

To investigate the toxic effects of RICP, we performed in vitro cytotoxicity studies of RICP (Fig. S23, ESI†). The results showed that RICP did not exhibit significant toxicity to HUVEC and RAW264.7 cells. Moreover, RICP administration did not cause significant changes in serum alanine aminotransferase (ALT) and aspartate aminotransferase (AST) levels in mice, suggesting negligible liver burden (Fig. S24, ESI†).

## 3.3 RICP-induced antigen-specific immune tolerance to model antigens

Enzyme replacement therapy (ERT) has long been used to treat the loss of function of specific proteins associated with rare diseases.<sup>57</sup> Data from clinical and preclinical animal models suggest that high anti-drug antibody titers (ADAs) against recombinant proteins affect efficacy. It is representative that whether RICP would prevent antibody response against uricase, an enzyme limited by immunogenicity. Mice were treated with various formulations co-administrated with uricase and then

re-challenged with uricase after the tolerance period weekly (Fig. 3(A)). Mice treated with free ITA exhibited no effect in the total period, while the free RAPA group and the free RAPA plus ITA group showed a slight antibody inhibition response on day 21 and day 28, but showed a rapid recovery antibody response on day 35 and day 42 after three challenge injections of uricase alone (Fig. 3(B)-(I)). This delayed response indicated that free RAPA only exerted a transient immune suppression but not durable immune tolerance. It is noteworthy that the free RAPA-C<sub>10</sub> plus ITA-C<sub>18</sub> group exhibited positive effects to some extent by reducing anti-uricase antibodies. This may be attributed to their structure having a hydrophobic long chain that helps to prolong its half-life. In contrast, mice treated with three weekly injections of uricase plus RICP showed durable immune tolerance to uricase, which remained on day 42 at least compared to the above-mentioned free drug groups (Fig. 3(B)-(I)).

To assess whether RICP could induce antigen-specific immunological tolerance, and not just systemic immunosuppression, mice were treated with three intravenous injections of RICP, coadministrated with KLH, and then challenged with KLH and unrelated protein ovalbumin (OVA) after the weekly tolerance period (Fig. 4(A)). The results showed that the mice injected with KLH alone had a strong immune response to KLH, with a high level of anti-KLH IgG antibodies (Fig. 4(B)). The mice injected with RICP and KLH significantly blocked the development of anti-KLH responses. It demonstrated that this reduction in antibody response is due to the RICP, which is consistent across immunogenic antigens (Uricase and KLH). Yet, mice tolerant to KLH by injections of RICP showed a normal response to OVA, similar to that of the mice treated with three injections of KLH alone, indicating that injections of RICP did not shown chronic immunosuppression (Fig. 4(C)). Together these data show that RICP, but not free RAPA or ITA or their free lipid derivatives, could induce durable and specific immunological tolerance when co-administered with the antigen.

#### 3.4 RICP treatment allowed for AAV vector re-administration

The ability to re-dose AAV would be important for enabling dose titration of AAV therapies to mitigate toxicities associated with high vector doses. We next evaluated the ability of RICP to enable a boost in transgene expression following a repeat dose of AAV vector administered three weeks after the initial treatment. Specifically, mice were injected first with an AAV8 vector encoding Luc together with RICP on day 0, followed by the second administration of an AAV8 vector encoding for Luc to monitor the transgene expression level by IVIS imaging or the second administration of an AAV8 vector encoding for the GFP to visualize transgene expression in the liver (Fig. 4(D)). The fluorescence expression results suggested that the animals injected with AAV8-Luc alone showed little further expression of the target transgene. Notably, coadministration of RICP with AAV8-Luc resulted in a 2-fold increase in hepatic luciferase expression compared to AAV8-Luc alone after the second dose (Fig. 4(E) and (F)). Moreover, the quantitation of the Luc activity quantification almost doubled after the second AAV stimulation compared to the mice treated with AAV8 alone (Fig. 4(G)).

Communication Materials Horizons

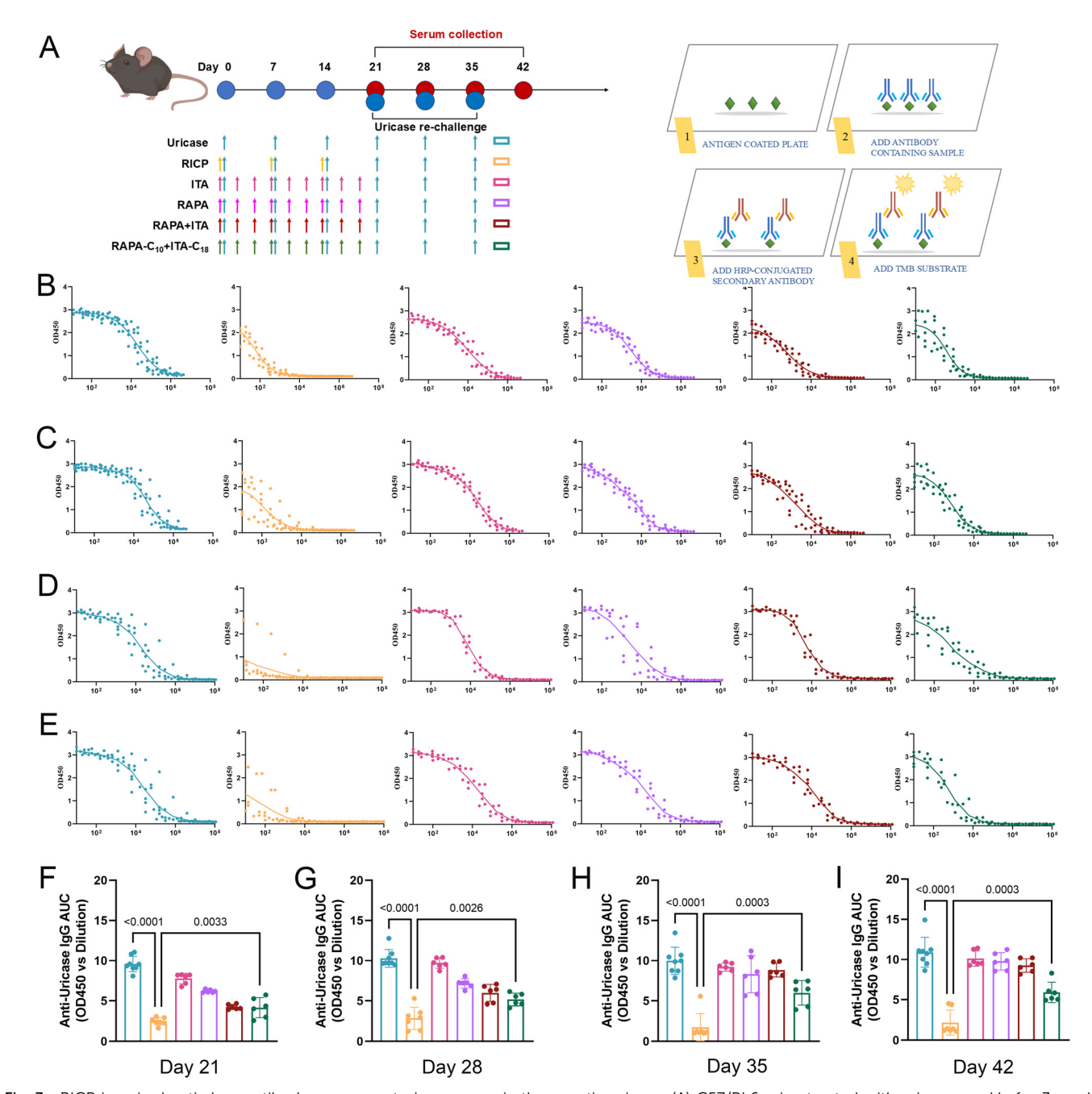


Fig. 3 RICP impaired anti-drug antibody responses to immunogenic therapeutic uricase. (A) C57/BL6 mice treated with uricase weekly for 3 weeks combined with RICP (3 times), free ITA (9 times), free RAPA (9 times), RAPA + ITA (9 times), RAPA- $C_{10}$  + ITA- $C_{18}$  (9 times) or saline followed by a therapeutic dose of uricase weekly for 3 weeks. (B)–(E) Anti-uricase IgG antibody levels (OD450 vs. dilution) showed on day 21, 28, 35 and 42 of various formulations, respectively. (F)–(I) Time course of the anti-uricase IgG antibody response of various formulations represented as the area under the curve of absorbance vs. log-transformed dilution (AUC) shown on day 21, 28, 35 and 42, respectively.

Hepatocytes positive for GFP were more detected in animals injected with AAV8-GFP together with RICP for the second time compared to the control animal (Fig. 4(H)).

Similar results were observed using AAV8-SEAP (Fig. 5(A)). Mice treated with AAV8-SEAP plus RICP showed an increased one-fold expression of SEAP, compared to mice treated with AAV8-SEAP alone, which showed almost no change in transgene expression after repeated dosing at week 6 (Fig. 5(B)). Furthermore, SEAP mRNA levels were quantified in the liver

and were significantly elevated in mice treated with RICP compared to animals treated with the AAV8-SEAP alone (Fig. 5(C)).

# 3.5 RICP induces the differentiation of Treg and inhibits the maturation of B cells through Tfh cells

As Fig. 5(D) and Fig. S25 (ESI†) show, RICP substantially suppressed anti-AAV IgG antibodies and remained low through Day 42 compared to control mice treated with AAV8 alone. More importantly, RICP demonstrated sustained and significant

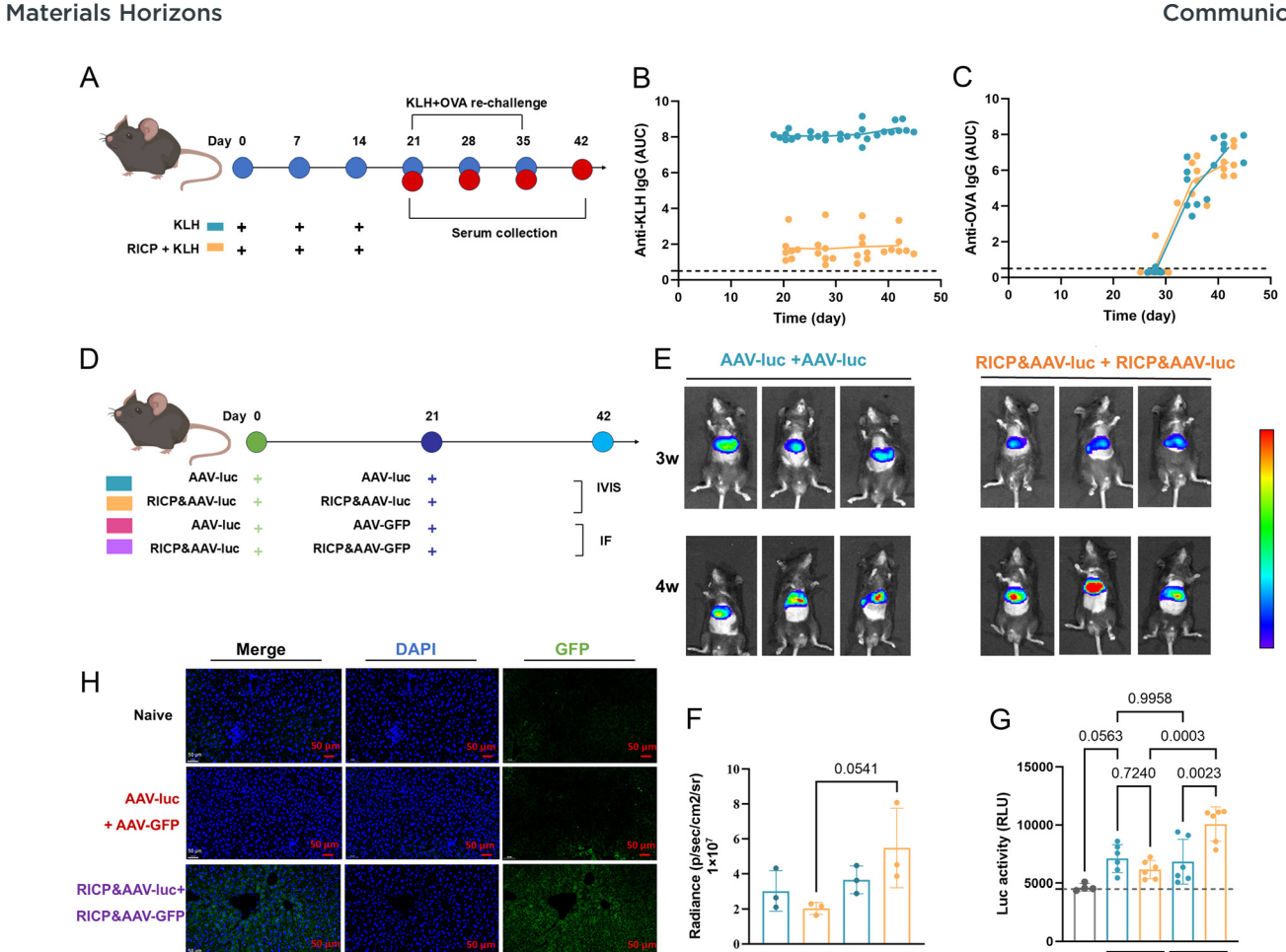


Fig. 4 Specificity of tolerance induced by RICP in combination with a free antigen. (A) Schematic of antigen-specific (KLH and OVA) tolerance induction. (B) and (C) Time course of anti-KLH IgG and anti-OVA IgG antibody response represented as the area under the curve of absorbance vs. log-transformed dilution (AUC), respectively. (D) C57BL/6 mice were treated intravenously with  $4 \times 10^{12}$  vg kg $^{-1}$  of AAV8-Luc together with RICP or with saline control. Three weeks later, animals were administered with  $4 \times 10^{12}$  vg kg $^{-1}$  of AAV8-Luc or AAV8-GFP vector together with either RICP or saline control. (E) and (F) In vivo bioluminescence imaging and quantification of mice on week 3 and week 4. (G) Luc expression levels in groups treated with AAV-Luc + RICP or with AAV-Luc alone. Gray bar represents that the Luc expression of wild mice. (H) Fluorescence of GFP and DAPI in the livers from mice treated with AAV8 vectors together with RICP or saline.

suppression of Nabs (Fig. S26 and S27, ESI†). Marginal zone B cells and B1 B cells in the mouse can produce IgM antibodies, which were demonstrated to be capable of neutralizing AAV transduction both in vitro and in vivo in the early stage of immune responses. Therefore, we also tested the anti-AAV8 IgM level in both RICP-treated and untreated animals. The treatment group showed partial inhibitory effect of IgM antibodies compared to the control group on day 7 after the first dose (Fig. 5(E)). These results indicated that RICP efficiently inhibited the anti-AAV8 antibody formation, allowing for vector re-dosing and effectively enhancing the gene expression.

To further investigate the mechanism responsible for the antibody inhibition effects triggered by RICP, the immune cells in the peripheral immune organ were analyzed by flow cytometry (FACS) on day 42 after the initial injection. We observed that the population of Tregs significantly increased after the administration of RICP in the lymph nodes and spleen compared to that in either the untreated group or the vector alone group (Fig. 5(F) and (G)). Moreover, the frequency of CXCR5<sup>+</sup>PD1<sup>+</sup> follicular helper T cells showed a decrease in RICP-mediated immunomodulation (Fig. 5(H)). Previous reports revealed that the inhibition of mTORc1 activity had a minimal impact on the generation of Tfh cells. Although a few research groups observed the suppression of Tfh cells after RAPA-treatment, further experiments revealed that reduced Tfh cell formation in rapamycin-treated mice was due to lower GC B cell responses, rather than acting directly on Tfh cells.<sup>58</sup>

We next evaluated the effect of RICP on B cells in vivo. Compared to untreated animals, mice treated with RICP showed a distinct reduction in the number of GC B cells, memory B cells and plasma cells (Fig. 5(I)-(K)) relative to the mice injected with AAV8 alone. The observed reduction in B-cell differentiation implies a potential impairment in antibody production capacity in RICP-treated mice, as evidenced by significantly diminished AAV8 vector-specific IgM and IgG antibody responses compared to vehicle-treated controls. Taken together, these data demonstrate that RICP can effectively inhibit B-cell differentiation and antibody production.

Communication **Materials Horizons** 

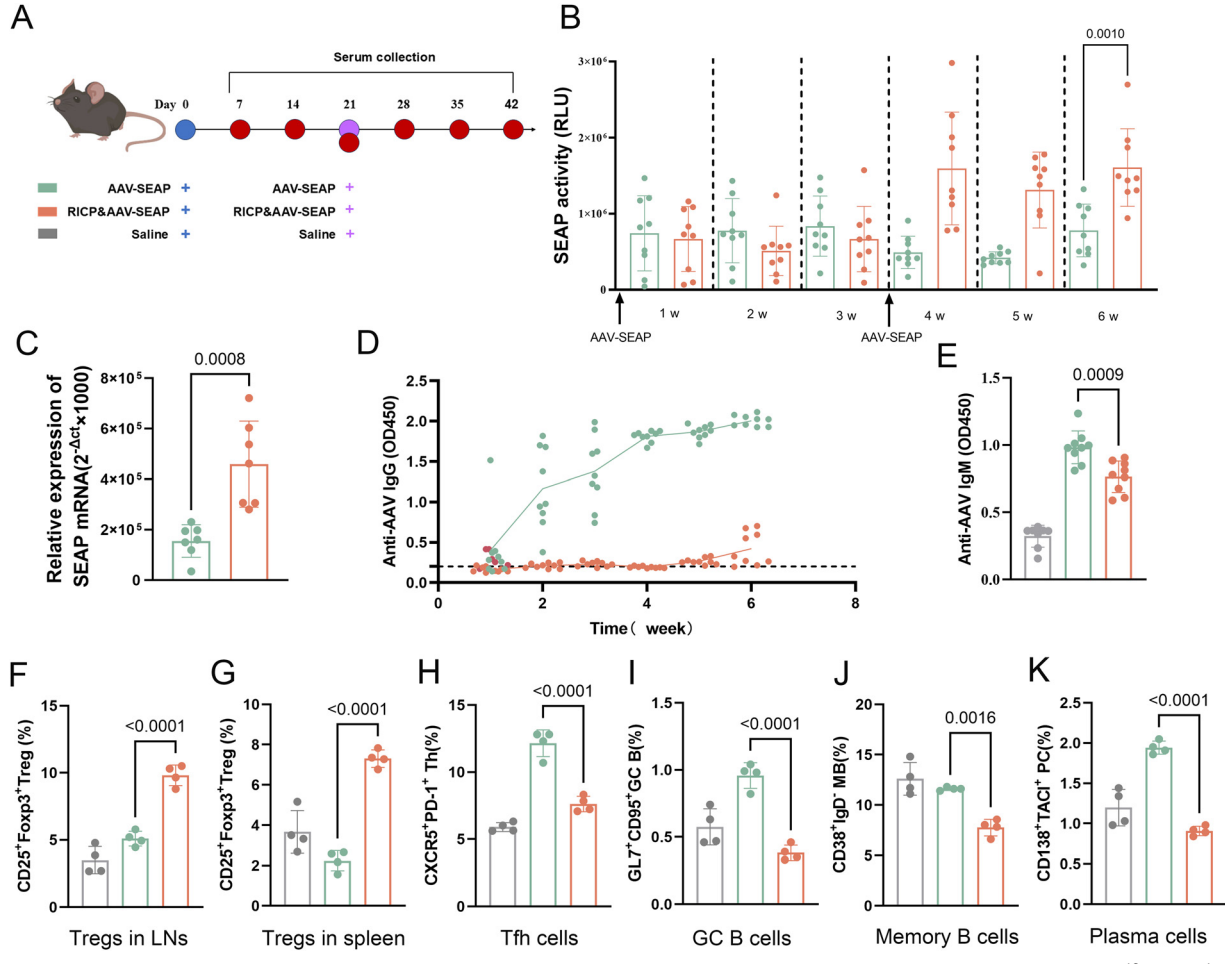


Fig. 5 Prevention of anti-AAV antibodies and cellular response to RICP in mice. (A) C57BL/6 mice treated intravenously with  $4 \times 10^{12}$  vg kg $^{-1}$  of AAV8-SEAP together with RICP or with saline control. Three weeks later, animals were administered with  $4 \times 10^{12}$  vg kg $^{-1}$  of AAV8-SEAP vector together with either RICP or saline control. (B) Quantification of SEAP activity level represented in groups treated with AAV-SEAP + RICP or with AAV-SEAP alone. (C) Viral mRNA from the second injection of AAV-SEAP measured in the liver. (D) Anti-AAV8 IgG antibody levels at indicated time points measured using ELISA. (E) Anti-AAV8 IgM antibody levels at week 1. (F) Quantitative analysis of CD25+Foxp3+ T cells in the lymph node. (G) Quantitative analysis of CD25+Foxp3+T cells in the spleen. (H)-(K) Quantitative analysis of follicular helper T cells (CXCR+PD-1+), germinal center B cells (GL-7+CD95+), memory B cells (CD38<sup>+</sup>IgD<sup>-</sup>) and plasma cells (CD138<sup>+</sup>TACI<sup>+</sup>).

## 4. Discussion

The therapeutic strategies described in this study take advantage of impairing CD4<sup>+</sup> T follicular helper cell collaboration by ITA and the formation of the Treg cells relying on inducing a tolerogenic phenotype in APCs by RAPA, by a facile carrier-free nano-system for synergistically inhibiting humoral immune response against AAV vectors.

Although previous reports have showed that the coadministration of RAPA-loaded PLGA/PLA NPs with pegloticase was evaluated to prevent the formation of antibodies in the clinic trials (NCT02464605, NCT02648269, NCT03905512), it is not clear whether RAPA NPs works in enabling re-dosing of AAV in human.<sup>59,60</sup> Several pathways including the TLR9/MyD88-IFN-γ cascade, complement activation, pre-existing antibody responses and T-cell response are shown to impact a wide range of biological processes for AAV administration. In addition, Li et al. have recently highlighted that unstable Treg cells transform

a effector-like phenotype in response to inflammation.<sup>24</sup> In human patients with a complex inflammation environment, such as infection, inflammation or tissue damage, the formation of the Treg cells by inducing a tolerogenic phenotype in APCs by RAPA alone is not as reliable as once thought.

The feedback loops of Tfh cells and GC B cells are central aspects of proper regulation of humoral immunity. Tfh cells are critical regulators of long-term humoral immunity via GC B cell differentiation to memory B cells. Immunological memory is a critical factor primed to overcome the challenge of AAV readministration, essentially acting as a vaccine against readministration of the AAV therapy if required and reducing the therapeutic transduction efficiency. Besides, the activation of this memory response does not require an innate immune response. Herein, we provide a proof of concept to block T helper cells (Tfh cells and Th2 cells) and B cell collaboration as an emerging immune regulation to replenish the method of expansion of Tregs by RAPA to act synergistically to abolish

memory humoral immune responses for enabling AAV readministration. While IL-10 upregulation and in vivo immunomodulatory effects support Treg functionality, future work will include direct suppression assays (e.g., effector T-cell proliferation) and in vivo depletion or adoptive-transfer studies to conclusively define the stability and suppressive capacity of RICP-induced Tregs.

Indeed, CD4<sup>+</sup> T helper cells remain a promising target for regulating humoral immune response. For instance, Alameh et al. indicated that induction of strong T follicular helper cells was associated with durable and protective antibodies in mice. 61 In humans, Norihide et al. attributed the lower peak IgG levels and compromised immune response to the delayed induction of CD4<sup>+</sup> helper T cell responses after the mRNA COVID-19 vaccination.<sup>62</sup> However, it is unclear whether CD4<sup>+</sup> helper T cells play a more critical role in enabling AAV readministration. Our studies revealed that RICP not only block the formation of the Th2 cells in vitro, but also inhibit the generation of the Tfh cells in vivo after injection of the AAV. We also showed that RICP together with AAV vectors can significantly increase the expression of a transgene (such as Luc, GFP and SEAP) in the liver at re-dosing, compared to mice treated with AAV alone, which showed almost no change in transgene expression.

This study has several limitations. First, we did not analyze APCs that are also critical for AAV re-administration in vivo, although this has been well demonstrated in other studies. Second, since it is difficult to obtain *in vitro* real Tfh cells, only Th2 cells were used to evaluate RICP in vitro. Third, we evaluated only anti-AAV IgG and IgM antibody titers but not neutralizing activity, although these two parameters are highly correlated.

In conclusion, we showed that RICP can abolish the undesired humoral immune response against AAV vectors through acting synergistically on DC-Treg and Tfh-B cell axis. Specifically, the decreased induction of Tfh cells may provide a useful (although incomplete) proxy for the lower memory B cells, which are critical for the development of long-term humoral immunity and obstacle for AAV re-administration. This study provided insights into the development of AAV gene therapy with higher efficacy and the establishment of a readministration schedule suitable for re-storing therapeutic benefits in patients not only with initial treatment failure, but also in the presence of significant cell proliferation, such as in children. In summary, the convergence of nanotechnology and immune tolerance exhibits remarkable technical merits and holds immense potential for practical applications. 63,64

## Author contributions

Yubo Liu: conceptualization, methodology, writing - original draft. Fangming Liang: methodology. Rui Zhang: methodology. Chengcheng Tang: methodology. Xin Li: methodology. Yongjun Wang: supervision. Zhonggui He: supervision. Hongzhuo Liu: conceptualization, writing - review & editing.

## Data availability

The data that support the findings of this study are available from the corresponding author [e-mail: liuhongzhuo@syphu.edu.cn] upon reasonable request.

## Conflicts of interest

The authors declare no conflict of interest.

## Acknowledgements

This work was supported by the Department of Education of Liaoning Province (no. LJKMZ20221357) and Shenyang Municipal Bureau of Science and Technology (no. 23-503-6-11).

## References

- 1 A. Pupo, A. Fernández, S. H. Low, A. François, L. Suárez-Amarán and R. J. Samulski, AAV vectors: The Rubik's cube of human gene therapy, Mol. Ther., 2022, 30(12), 3515-3541.
- 2 M. Arjomandnejad, I. Dasgupta, T. R. Flotte and A. M. Keeler, Immunogenicity of Recombinant Adeno-Associated Virus (AAV) Vectors for Gene Transfer, BioDrugs, 2023, 37(3),
- 3 J. Earley, E. Piletska, G. Ronzitti and S. Piletsky, Evading and overcoming AAV neutralization in gene therapy, Trends Biotechnol., 2023, 41(6), 836-845.
- 4 A. Gardin and G. Ronzitti, Current limitations of gene therapy for rare pediatric diseases: Lessons learned from clinical experience with AAV vectors, Arch. Pediatr., 2023, 30(8), 8S46-8S52.
- 5 F. Mingozzi and K. A. High, Immune responses to AAV vectors: overcoming barriers to successful gene therapy, Blood, 2013, 122(1), 23-36.
- 6 J. Rabinowitz, Y. K. Chan and R. J. Samulski, Adeno-Associated Virus (AAV) Versus Immune Response, Viruses, 2019, 11(2), 102.
- 7 H. C. Verdera, K. Kuranda and F. Mingozzi, AAV Vector Immunogenicity in Humans: A Long Journey to Successful Gene Transfer, Mol. Ther., 2020, 28(3), 723-746.
- 8 T.-L. Wu and H. C. J. Ertl, Immune barriers to successful gene therapy, Trends Mol. Med., 2009, 15(1), 32-39.
- 9 E. Kropf, D. M. Markusic, A. Majowicz, F. Mingozzi and K. Kuranda, Complement System Response to Adeno-Associated Virus Vector Gene Therapy, Hum. Gene Ther., 2024, 35(13-14), 425-438.
- 10 C. West, J. D. Federspiel, K. Rogers, A. Khatri, S. Rao-Dayton, M. F. Ocana, S. Lim, A. M. D'Antona, S. Casinghino and S. Somanathan, Complement Activation by Adeno-Associated Virus-Neutralizing Antibody Complexes, Hum. Gene Ther., 2023, 34(11-12), 554-566.
- 11 F. Mingozzi, Y. Chen, S. C. Edmonson, S. Zhou, R. M. Thurlings, P. P. Tak, K. A. High and M. J. Vervoordeldonk, Prevalence and pharmacological modulation of humoral

immunity to AAV vectors in gene transfer to synovial tissue, *Gene Ther.*, 2013, 20(4), 417–424.

Communication

- 12 F. Mingozzi, N. C. Hasbrouck, E. Basner-Tschakarjan, S. A. Edmonson, D. J. Hui, D. E. Sabatino, S. Zhou, J. F. Wright, H. Jiang, G. F. Pierce, V. R. Arruda and K. A. High, Modulation of tolerance to the transgene product in a nonhuman primate model of AAV-mediated gene transfer to liver, *Blood*, 2007, 110(7), 2334–2341.
- 13 H. T. Le, Q. C. Yu, J. M. Wilson and M. A. Croyle, Utility of PEGylated recombinant adeno-associated viruses for gene transfer, *J. Controlled Release*, 2005, **108**(1), 161–177.
- 14 T. Yao, X. Zhou, C. Zhang, X. Yu, Z. Tian, L. Zhang and D. Zhou, Site-Specific PEGylated Adeno-Associated Viruses with Increased Serum Stability and Reduced Immunogenicity, *Molecules*, 2017, 22(7), 1155.
- 15 B. Bertin, P. Veron, C. Leborgne, J.-Y. Deschamps, S. Moullec, Y. Fromes, F. Collaud, S. Boutin, V. Latournerie, L. van Wittenberghe, B. Delache, R. Le Grand, N. Dereuddre-Bosquet, O. Benveniste, P. Moullier, C. Masurier, O. Merten and F. Mingozzi, Capsid-specific removal of circulating antibodies to adeno-associated virus vectors, *Sci. Rep.*, 2020, 10(1), 864.
- 16 F. Mingozzi, X. M. Anguela, G. Pavani, Y. Chen, R. J. Davidson, D. J. Hui, M. Yazicioglu, L. Elkouby, C. J. Hinderer, A. Faella, C. Howard, A. Tai, G. M. Podsakoff, S. Zhou, E. Basner-Tschakarjan, J. F. Wright and K. A. High, Overcoming Preexisting Humoral Immunity to AAV Using Capsid Decoys, Sci. Transl. Med., 2013, 5(194), 194ra92.
- 17 D. Dalkara, L. C. Byrne, R. R. Klimczak, M. Visel, L. Yin, W. H. Merigan, J. G. Flannery and D. V. Schaffer, In Vivo-Directed Evolution of a New Adeno-Associated Virus for Therapeutic Outer Retinal Gene Delivery from the Vitreous, *Sci. Transl. Med.*, 2013, 5(189), 189ra76.
- 18 L. V. Tse, K. A. Klinc, V. J. Madigan, R. M. C. Rivera, L. F. Wells, L. P. Havlik, J. K. Smith, M. Agbandje-McKenna and A. Asokan, Structure-guided evolution of antigenically distinct adeno-associated virus variants for immune evasion, *Proc. Natl. Acad. Sci. U. S. A.*, 2017, 114(24), E4812–E4821.
- 19 R. P. Wallace, K. C. Refvik, J. T. Antane, K. Brünggel, A. C. Tremain, M. R. Raczy, A. T. Alpar, M. Nguyen, A. Solanki, A. J. Slezak, E. A. Watkins, A. L. Lauterbach, S. Cao, D. S. Wilson and J. A. Hubbell, Synthetically mannosylated antigens induce antigen-specific humoral tolerance and reduce anti-drug antibody responses to immunogenic biologics, Cell Rep. Med., 2024, 5(1), 101345.
- 20 T. K. Kishimoto, J. D. Ferrari, R. A. LaMothe, P. N. Kolte, A. P. Griset, C. O'Neil, V. Chan, E. Browning, A. Chalishazar, W. Kuhlman, F.-n Fu, N. Viseux, D. H. Altreuter, L. Johnston and R. A. Maldonado, Improving the efficacy and safety of biologic drugs with tolerogenic nanoparticles, *Nat. Nanotechnol.*, 2016, 11(10), 890–899.
- 21 A. Meliani, F. Boisgerault, R. Hardet, S. Marmier, F. Collaud, G. Ronzitti, C. Leborgne, H. Costa Verdera, M. Simon Sola, S. Charles, A. Vignaud, L. van Wittenberghe, G. Manni, O. Christophe, F. Fallarino, C. Roy, A. Michaud, P. Ilyinskii, T. K. Kishimoto and F. Mingozzi, Antigen-selective

- modulation of AAV immunogenicity with tolerogenic rapamycin nanoparticles enables successful vector re-administration, *Nat. Commun.*, 2018, **9**(1), 4098.
- 22 S. L. Bailey-Bucktrout, M. Martinez-Llordella, X. Zhou, B. Anthony, W. Rosenthal, H. Luche, H. J. Fehling and J. A. Bluestone, Self-antigen-Driven Activation Induces Instability of Regulatory T Cells during an Inflammatory Autoimmune Response, *Immunity*, 2013, 39(5), 949–962.
- 23 N. Komatsu, K. Okamoto, S. Sawa, T. Nakashima, M. Oh-hora, T. Kodama, S. Tanaka, J. A. Bluestone and H. Takayanagi, Pathogenic conversion of Foxp3+ T cells into TH17 cells in autoimmune arthritis, *Nat. Med.*, 2013, **20**(1), 62–68.
- 24 Y. Li, Y. Lu, S. Wang, Z. Han, F. Zhu, Y. Ni, R. Liang, Y. Zhang, Q. Leng, G. Wei, G. Shi, R. Zhu, D. Li, H. Wang, S. G. Zheng, H. Xu, A. Tsun and B. Li, USP21 prevents the generation of T-helper-1-like Treg cells, *Nat. Commun.*, 2016, 7, 13559.
- 25 S. Crotty, T Follicular Helper Cell Biology: A Decade of Discovery and Diseases, *Immunity*, 2019, **50**(5), 1132–1148.
- 26 L. Almeida, M. Lochner, L. Berod and T. Sparwasser, Metabolic pathways in T cell activation and lineage differentiation, *Semin. Immunol.*, 2016, **28**(5), 514–524.
- 27 S. Crotty, T Follicular Helper Cell Differentiation, Function, and Roles in Disease, *Immunity*, 2014, 41(4), 529–542.
- 28 C. Dong, Cytokine Regulation and Function in T Cells, *Annu. Rev. Immunol.*, 2021, **39**(1), 51–76.
- 29 C. L. Mayberry, N. A. Logan, J. J. Wilson and C.-H. Chang, Providing a Helping Hand: Metabolic Regulation of T Follicular Helper Cells and Their Association With Disease, Front. Immunol., 2022, 13, 864949.
- 30 K. J. Oestreich, K. A. Read, S. E. Gilbertson, K. P. Hough, P. W. McDonald, V. Krishnamoorthy and A. S. Weinmann, Bcl-6 directly represses the gene program of the glycolysis pathway, *Nat. Immunol.*, 2014, **15**(10), 957–964.
- 31 J. M. Stark, C. A. Tibbitt and J. M. Coquet, The Metabolic Requirements of Th2 Cell Differentiation, *Front. Immunol.*, 2019, **10**, 2318.
- 32 X. Yin, S. Chen and S. C. Eisenbarth, Dendritic Cell Regulation of T Helper Cells, *Annu. Rev. Immunol.*, 2021, **39**(1), 759–790.
- 33 X. Zou, S.-C. Choi, L. Zeumer-Spataro, Y. Scindia, E. K. Moser and L. Morel, Metabolic regulation of follicular helper T cell differentiation in a mouse model of lupus, *Immunol. Lett.*, 2022, 247, 13–21.
- 34 H. Kato and A. Perl, Mechanistic Target of Rapamycin Complex 1 Expands Th17 and IL-4+ CD4-CD8- Double-Negative T Cells and Contracts Regulatory T Cells in Systemic Lupus Erythematosus, *J. Immunol.*, 2014, **192**(9), 4134-4144.
- 35 J. B. Mannick and D. W. Lamming, Targeting the biology of aging with mTOR inhibitors, *Nat. Aging*, 2023, 3(6), 642–660.
- 36 A. Perl, Activation of mTOR (mechanistic target of rapamycin) in rheumatic diseases, *Nat. Rev. Rheumatol.*, 2015, **12**(3), 169–182.
- 37 M. Battaglia, A. Stabilini and M.-G. Roncarolo, Rapamycin selectively expands CD4 + CD25 + FoxP3+ regulatory T cells, *Blood*, 2005, **105**(12), 4743–4748.

38 G. M. Delgoffe, K. N. Pollizzi, A. T. Waickman, E. Heikamp, D. J. Meyers, M. R. Horton, B. Xiao, P. F. Worley and J. D. Powell, The kinase mTOR regulates the differentiation of helper T cells through the selective activation of signaling by mTORC1 and mTORC2, Nat. Immunol., 2011, 12(4), 295-303.

**Materials Horizons** 

- 39 L. Almeida, A. Dhillon-LaBroov, G. Carriche, L. Berod and T. Sparwasser, CD4+ T-cell differentiation and function: Unifying glycolysis, fatty acid oxidation, polyamines NAD mitochondria, J. Allergy Clin. Immunol., 2021, 148(1), 16-32.
- 40 R. D. Michalek, V. A. Gerriets, S. R. Jacobs, A. N. Macintyre, N. J. MacIver, E. F. Mason, S. A. Sullivan, A. G. Nichols and J. C. Rathmell, Cutting Edge: Distinct Glycolytic and Lipid Oxidative Metabolic Programs Are Essential for Effector and Regulatory CD4+ T Cell Subsets, J. Immunol., 2011, 186(6), 3299-3303.
- 41 D. O'Sullivan and E. L. Pearce, Targeting T cell metabolism for therapy, Trends Immunol., 2015, 36(2), 71-80.
- 42 L. Z. Shi, R. Wang, G. Huang, P. Vogel, G. Neale, D. R. Green and H. Chi, HIF1α-dependent glycolytic pathway orchestrates a metabolic checkpoint for the differentiation of TH17 and Treg cells, J. Exp. Med., 2011, 208(7), 1367-1376.
- 43 K. Aso, M. Kono, M. Kanda, Y. Kudo, K. Sakiyama, R. Hisada, K. Karino, Y. Ueda, D. Nakazawa, Y. Fujieda, M. Kato, O. Amengual and T. Atsumi, Itaconate ameliorates autoimmunity by modulating T cell imbalance via metabolic and epigenetic reprogramming, Nat. Commun., 2023, **14**(1), 984.
- 44 A. K. Jaiswal, J. Yadav, S. Makhija, S. Mazumder, A. K. Mitra, A. Suryawanshi, M. Sandey and A. Mishra, Irg1/itaconate metabolic pathway is a crucial determinant of dendritic cells immune-priming function and contributes to resolute allergen-induced airway inflammation, Mucosal Immunol., 2022, **15**(2), 301–313.
- 45 S.-T. Liao, C. Han, D.-Q. Xu, X.-W. Fu, J.-S. Wang and L.-Y. Kong, 4-Octyl itaconate inhibits aerobic glycolysis by targeting GAPDH to exert anti-inflammatory effects, Nat. Commun., 2019, 10(1), 5091.
- 46 E. L. Mills, D. G. Ryan, H. A. Prag, D. Dikovskaya, D. Menon, Z. Zaslona, M. P. Jedrychowski, A. S. H. Costa, M. Higgins, E. Hams, J. Szpyt, M. C. Runtsch, M. S. King, J. F. McGouran, R. Fischer, B. M. Kessler, A. F. McGettrick, M. M. Hughes, R. G. Carroll, L. M. Booty, E. V. Knatko, P. J. Meakin, M. L. J. Ashford, L. K. Modis, G. Brunori, D. C. Sévin, P. G. Fallon, S. T. Caldwell, E. R. S. Kunji, E. T. Chouchani, C. Frezza, A. T. Dinkova-Kostova, R. C. Hartley, M. P. Murphy and L. A. O'Neill, Itaconate is an anti-inflammatory metabolite that activates Nrf2 via alkylation of KEAP1, Nature, 2018, 556(7699), 113-117.
- 47 M. C. Runtsch, S. Angiari, A. Hooftman, R. Wadhwa, Y. Zhang, Y. Zheng, J. S. Spina, M. C. Ruzek, M. A. Argiriadi, A. F. McGettrick, R. S. Mendez, A. Zotta, C. G. Peace, A. Walsh, R. Chirillo, E. Hams, P. G. Fallon, R. Jayaraman, K. Dua, A. C. Brown, R. Y. Kim, J. C. Horvat, P. M. Hansbro, C. Wang and L. A. J. O'Neill, Itaconate and itaconate derivatives target JAK1 to suppress alternative activation of macrophages, Cell Metab., 2022, 34(3), 487-501.

- 48 T. A. J. Ryan, A. Hooftman, A. M. Rehill, M. D. Johansen, E. C. O. Brien, J. E. Toller-Kawahisa, M. M. Wilk, E. A. Day, H. J. Weiss, P. Sarvari, E. G. Vozza, F. Schramm, C. G. Peace, A. Zotta, S. Miemczyk, C. Nalkurthi, N. G. Hansbro, G. McManus, L. O'Doherty, S. Gargan, A. Long, J. Dunne, C. N. Cheallaigh, N. Conlon, M. Carty, P. G. Fallon, K. H. G. Mills, E. M. Creagh, J. S. O. Donnell, P. J. Hertzog, P. M. Hansbro, R. M. McLoughlin, M. Wygrecka, R. J. S. Preston, Z. Zasłona and L. A. J. O'Neill, Dimethyl fumarate and 4-octyl itaconate are anticoagulants that suppress Tissue Factor in macrophages via inhibition of Type I Interferon, Nat. Commun., 2023, 14(1), 3513.
- X. Shi, H. Zhou, J. Wei, W. Mo, Q. Li and X. Lv, The signaling pathways and therapeutic potential of itaconate to alleviate inflammation and oxidative stress in inflammatory diseases, Redox Biol., 2022, 58, 102553.
- 50 A. Swain, M. Bambouskova, H. Kim, P. S. Andhey, D. Duncan, K. Auclair, V. Chubukov, D. M. Simons, T. P. Roddy, K. M. Stewart and M. N. Artyomov, Comparative evaluation of itaconate and its derivatives reveals divergent inflammasome and type I interferon regulation in macrophages, Nat. Metab., 2020, 2(7), 594-602.
- 51 Z. Zhang, C. Chen, F. Yang, Y.-X. Zeng, P. Sun, P. Liu and X. Li, Itaconate is a lysosomal inducer that promotes antibacterial innate immunity, Mol. Cell, 2022, 82(15), 2844-2857.
- 52 H. Zhao, D. Teng, L. Yang, X. Xu, J. Chen, T. Jiang, A. Y. Feng, Y. Zhang, D. T. Frederick, L. Gu, L. Cai, J. M. Asara, M. Pasca di Magliano, G. M. Boland, K. T. Flaherty, K. D. Swanson, D. Liu, J. D. Rabinowitz and B. Zheng, Myeloid-derived itaconate suppresses cytotoxic CD8+ T cells and promotes tumour growth, Nat. Metab., 2022, 4(12), 1660-1673.
- 53 C. Gan, M. Leng, Y. Liu, Z. Zheng, S. He, W. Qiao, L. Xiao, Y. Xiao, J. Ye, L. Zhou, J. Zhou, B. Xiao, W. Zhao, J. Yang, A. Wu, H. Zhang, H. Hu, X. Cen, Z. Qian, H. Dong, C. A. Valencia, L. Dai, H. Y. Chow, L. Zhang and B. Dong, The combination of rAAV pseudo-lipid nanoparticle and triamcinolone acetonide enables multi-administration to liver, Mol. Ther.-Methods Clin. Dev., 2025, 33(1), 101399.
- 54 A. Meliani, C. Leborgne, S. Triffault, L. Jeanson-Leh, P. Veron and F. Mingozzi, Determination of Anti-Adeno-Associated Virus Vector Neutralizing Antibody Titer with an In Vitro Reporter System, Hum. Gene Ther: Methods, 2015, 26(2), 45-53.
- 55 L. B. Ivashkiv and L. T. Donlin, Regulation of type I interferon responses, Nat. Rev. Immunol., 2013, 14(1), 36-49.
- 56 A. Sahoo, S. Wali and R. Nurieva, Thelper 2 and T follicular helper cells: Regulation and function of interleukin-4, Cytokine Growth Factor Rev., 2016, 30, 29-37.
- 57 M. Lenders and E. Brand, Mechanisms of Neutralizing Antidrug Antibody Formation and Clinical Relevance on Therapeutic Efficacy of Enzyme Replacement Therapies in Fabry Disease, Drugs, 2021, 81(17), 1969–1981.
- 58 L. Ye, J. Lee, L. Xu, A.-U.-R. Mohammed, W. Li, J. S. Hale, W. G. Tan, T. Wu, C. W. Davis, R. Ahmed and K. Araki,

mTOR Promotes Antiviral Humoral Immunity by Differen-

Communication

- tially Regulating CD4 Helper T Cell and B Cell Responses, J. Virol., 2017, 91(4), e01653-16.
- 59 H. S. B. Baraf, P. P. Khanna, A. J. Kivitz, V. Strand, H. K. Choi, R. Terkeltaub, N. Dalbeth, W. DeHaan, R. Azeem, P. G. Traber and R. T. Keenan, The COMPARE head-to-head, randomized controlled trial of SEL-212 (pegadricase plus rapamycin-containing nanoparticle, ImmTOR™) versus pegloticase for refractory gout, Rheumatology, 2024, 63(4), 1058-1067.
- 60 E. Sands, A. Kivitz, W. DeHaan, S. S. Leung, L. Johnston and T. K. Kishimoto, Tolerogenic nanoparticles mitigate the formation of anti-drug antibodies against pegylated uricase in patients with hyperuricemia, Nat. Commun., 2022, 13(1), 272.
- 61 M.-G. Alameh, I. Tombácz, E. Bettini, K. Lederer, S. Ndeupen, C. Sittplangkoon, J. R. Wilmore, B. T. Gaudette, O. Y. Soliman, M. Pine, P. Hicks, T. B. Manzoni, J. J. Knox, J. L. Johnson, D. Laczkó, H. Muramatsu, B. Davis, W. Meng, A. M. Rosenfeld, S. Strohmeier, P. J. C. Lin, B. L. Mui, Y. K. Tam,

- K. Karikó, A. Jacquet, F. Krammer, P. Bates, M. P. Cancro, D. Weissman, E. T. Luning Prak, D. Allman, B. Z. Igyártó, M. Locci and N. Pardi, Lipid nanoparticles enhance the efficacy of mRNA and protein subunit vaccines by inducing robust T follicular helper cell and humoral responses, Immunity, 2021, 54(12), 2877-2892.
- 62 N. Jo, Y. Hidaka, O. Kikuchi, M. Fukahori, T. Sawada, M. Aoki, M. Yamamoto, M. Nagao, S. Morita, T. E. Nakajima, M. Muto and Y. Hamazaki, Impaired CD4+ T cell response in older adults is associated with reduced immunogenicity and reactogenicity of mRNA COVID-19 vaccination, Nat. Aging, 2023, 3(1), 82-92.
- 63 J. Jiang, X. Cui, Y. Huang, D. Yan, B. Wang, Z. Yang, M. Chen, J. Wang, Y. Zhang, G. Liu, C. Zhou, S. Cui, J. Ni, F. Yang and D. Cui, Advances and Prospects in Integrated Nano-oncology, Nano Biomed. Eng., 2024, 16(2), 152-187.
- 64 X. Zhu, Y. Li and N. Gu, Application of Artificial Intelligence in the Exploration and Optimization of Biomedical Nanomaterials, Nano Biomed. Eng., 2023, 15(3), 342-353.